Inverse-designed terahertz modulators based on semiconductor multilayers

E Centeno, E Alvear-Cabezón, Rafik Smaali, A Moreau, T Taliercio

Inverse-designed terahertz modulators based on semiconductor multilayers

E. Centeno[1], E. Alvear-Cabezón[1], R. Smaali[1], A. Moreau[1], T. Taliercio[2]

[1] Université Clermont Auvergne, CNRS, SIGMA Clermont, Institut Pascal, F-63000 Clermont-Ferrand, France
[2] IES, Univ Montpellier, UMR CNRS 5214, Montpellier, FR

E-mail: emmanuel.centeno@uca.fr

Abstract. Using a global optimization algorithm, Differential Evolution, we show that optically actuated THz modulators can be designed using multilayers of InAs and GaSb semiconductors. The optical pump is actually able to generate photocarriers which diffuse into the structure and drastically modify its response at THz frequencies. A modulation depth between 63 % to 85 % is reached in the range of 1-3 THz for a low pump irradiance of 10 $W.cm^{-2}$ in the continuous regime, whether the modulators operate at one or up to four arbitrary chosen frequencies.

Keywords: Terahertz modulator, photogeneration, differential evolution algorithms

1. Introduction

Terahertz (THz) electromagnetic waves are expected to play a crucial role in several domains such as security, wireless communication, imaging, sensing [1, 2, 3, 4, 5]. Even if important milestones have been reached when it comes to THz sources and detectors [6, 7, 8], there is a pressing demand for versatile devices able to manipulate the amplitude or the phase of THz signals. Several approaches have been proposed to address the lack of adapted materials and of a clear path towards compact, cheap and efficient devices [9, 10, 11]. While the modulation speed and depth constitute the first performance indicators, it is highly desirable for a modulator to operate at room temperature, consume little energy and to be manufactured at low cost[12].

Metamaterial-based modulators have for example been used to enhance the interaction with the electromagnetic wave, achieving a large modulation and fast response in a narrow band of frequency. The resonant behavior of the metasurface can be modulated by applying different external stimuli such as a temperature change, an illumination or an electric field, thereby realizing the modulation of the THz waves [13, 14, 15, 16, 17, 18, 19, 20, 21]. Comparative studies of these approaches can be found in the latest references. However, such an approach relies on costly top-down fabrication processes. Recently, high electronics mobility transistors (HEMT) combined with metasurfaces have been proposed to increase the modulation speed [22, 23, 24, 25]. A 400 kHz 3 dB cut-off frequency has for instance been realized with a relative modulation depth of 90% over a spectrum bandwidth of 83 GHz (435.6-518.4 GHz) [26]. However, the performance of such devices is severely degraded at room temperature, reaching only a 30% modulation and thus preventing any easy on-chip integration.

Bulk semiconductors have also been investigated, because they offer the possibility to literally photo-generate metasurfaces. In this approach an optical pump creates carriers inside the semi-conductor, which will locally change its permittivity and thus its optical response. Well chosen illumination patterns allow to tailor the metasurface response. The modulation band can be largely broadened for these devices, allowing for the device to operate over a wide range of frequencies[27, 28, 29, 30, 31, 32]. A transient metasurface presenting a wide modulation band from 0.5 to 2 THz has been demonstrated with GaAs [33]. The main limitations of this approach come first from the optical pump power required to efficiently induces the refractive index change and then from the recombination time of the photocarriers which limits the modulation speed.

A review of the literature thus shows that for now, THz modulators rely on complex physical concepts making them difficult to design, because of a lot of nonlinear feedback. Furthermore, they are rather costly to fabricate. Recent results however suggest that InAs is an interesting candidate to realize an efficient modulation with a very low pump power [34]. An ultrathin epsilon-near-zero (ENZ) slab photo-generated in InAs semiconductor has presented a relative modulation depth of 90% at 1 THz with a continuous laser for an irradiation typically lower than 10 $W.cm^{-2}$ and a 3dB cut-off frequency of 2 MHz in the dynamic regime [35].

In this work, efficient optically actuated THz modulators based on multilayers alternating InAs and GaSb slabs are designed by the use of a Differential Evolution (DE) algorithm [36]. Single and multi-frequency modulators are demonstrated in the range of 0.5-5 THz with a low pump irradiance of 10 $W.cm^{-2}$ in the continuous regime. High modulation depth between 63 % to 85 % is reached in this range of frequency. The structures are simple to fabricate since they present only few layers (6 to 12 layers) and provide a versatile and cost effective platform.

In section II, we detail the physics of the modulator and how the response of the modulator in the THz range can be simulated. We extend the previous photogeneration theory detailed in [34] to the case of a more realistic nonlinear transport equation. We then detail our methodology regarding the design and introduce the optimization algorithm on which we rely on. In the last section, we present modulators working for a single or multiple wavelengths and discuss how these solutions can be physically understood, a key point to strengthen our confidence in the optimization results.

2. Physical principles and optimization methodology

2.1. Photogeneration in semiconductor multilayers

We consider a multilayered structure consisting of GaSb and InAs layers illuminated by a plane wave in

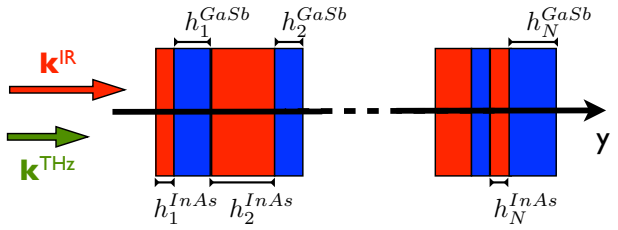

Figure 1. Scheme of the multilayered structure consisting of N InAs-GaSb pair of slabs. The infrared and THz plane waves progress toward the positive y-axis. The layers' thicknesses are denoted h_i^{InAs} and h_i^{GaAs}.

normal incidence at an infrared wavelength of 815 nm corresponding to the emission of a titanium-sapphire laser (see Fig. 1). This structure is surrounded with air. The permittivity of the GaSb semiconductor is described by a Lorentz model [37, 38] :

$$\epsilon^{GaSb} = \epsilon_\infty^{GaSb}\Big(1 + \frac{\Omega_{LO}^2 - \Omega_{TO}^2}{\omega_{TO}^2 - \omega^2 - i\omega\Gamma}\Big), \tag{1}$$

where the GaSb material parameters are $\epsilon_\infty^{GaSb} = 14.4$ $\Omega_{LO} = 43.9 \times 10^{12}\, rad/s$ $\Omega_{TO} = 42.2 \times 10^{12}\, rad/s$ $\Gamma = 0.56 \times 10^{12}\, rad/s$. At the infrared frequency, the GaSb layers can be considered a lossless dielectrics with a permittivity ϵ_∞^{GaSb} and consequently the pump field is only absorbed in the InAs layers which permittivity $\epsilon_{IR}^{InAs} = 13.64 + 3.3i$ at the 815 nm pump wavelength. Using a scattering matrix method for numerical reliability [39], we compute the electric field E_{IR} inside the structure for a pump irradiance denoted Φ_0:

$$E_{IR}(y) = \sqrt{2Z_0\Phi_0}E(y), \tag{2}$$

where Z_0 is the vacuum impedance and $E(y)$ the normalized electric field at the coordinate y.

This infrared pump irradiation generates carriers within the InAs layers whose density δn is governed by the ambipolar transport equation. In the steady state regime, this equation can be written

$$\frac{d^2\delta n}{dy^2} - \frac{\delta n}{L_a^2(\delta n)} = -\frac{G^{op}(y)}{D_a}. \tag{3}$$

The source term $G^{op}(y)$ of photogenerated electron-hole pairs is directly proportional to the absorption and can thus be written

$$G^{op}(y) = \pi/(hcZ_0)\Im(\varepsilon_{IR}) \mid E_{IR}(y) \mid^2, \tag{4}$$

where h the Planck's constant and c the speed of light in vacuum. This expression shows that the photocarriers are only generated inside the InAs layers since the imaginary part of GaSb permittivity is considered negligible. The photocarriers then diffuse within each InAs layers at a distance which depends on the ambipolar diffusion length defined by $L_a = \sqrt{D_a\tau_{eff}}$, where the ambipolar diffusion coefficient for InAs is $D_a = 23.5\, cm^2 s^{-1}$ at room temperature [40]. As often, surface recombination is neglected in the present study. Conversely to [34], the ambipolar diffusion length depends here on the effective recombination time of the photocarriers τ_{eff}, which takes into account three recombination processes: the Shockley-Read-Hall recombination (SRH), the radiative recombination and the Auger recombination [40]. The effective recombination rate can be expressed as a polynomial expansion:

$$\frac{1}{\tau_{eff}} = \frac{1}{\tau_{SRH}} + B\delta n + C\delta n^2, \tag{5}$$

where $\tau_{SRH} = 1.15 \times 10^{-6}$ s is the SRH recombination time, B is the radiative bimolecular recombination coefficient equal to $10^{-10}\, cm.s^{-1}$ and $C = 1.3 \times 10^{-28}\, cm^3.s^{-1}$ being the Auger coefficient [40]. From this equation, we plot the effective recombination time and the associated ambipolar diffusion length as a function of the carrier density, Fig. 2.

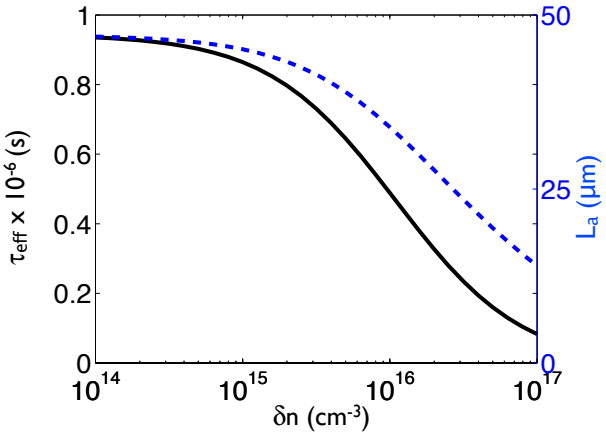

Figure 2. Effective recombination time and ambipolar diffusion lenght as functions of the photocarrier density.

Any increase in the density of photogenerated carriers results in a decrease of both τ_{eff} and L_a. Given the dependency of L_a on the carrier density, the ambipolar equation Equation (3) is highly non-linear. The pump irradiance monitors the carrier density which has an impact on the ambipolar diffusion length, which in turn has an impact on the carrier density, and so on. To solve this self-consistent problem, we assume that the carrier density is homogeneous inside each InAs layer. This approximation holds as long as the thicknesses of the InAs slabs are much smaller than the ambipolar diffusion length. Therefore, in this study, the maximum thickness for the InAs layers is set to 10 μm, 2 times smaller than L_a for the irradiance considered in this work. We then use an iterative algorithm to solve the ambipolar equation Equation (3). The procedure is initialized with an effective

recombination time $\tau_{eff}^{(0)} = \tau_{SRH}$. At iterative step (k), the ambipolar diffusion length is determined from $L_a^{(k)} = \sqrt{D_a \tau_{eff}^{(k)}}$. The carrier density $\delta_n^{(k)}$ is then calculated by solving the ambipolar equation thanks to a finite difference scheme. For iteration (k+1), a new value of the effective recombination time $\tau_{eff}^{(k+1)}$ is derived from Equation (5). This step is repeated until the condition $|\tau_{eff}^{(k+1)} - \tau_{eff}^{(k)}| < 10^{-10}$ is satisfied. The method converges in less than ten iterations.

The variations of the electronics density induced by the pump modify the electromagnetic response of the InAs layers at THz frequencies. In the THz range, the InAs relative permittivity is modeled by combining a Lorentz model for the phonon resonances and a Drude model to describe the contribution of the photocarriers [37, 38]:

$$\epsilon_m = \epsilon_\infty \Big(1 - \frac{\omega_p(n)^2}{\omega(\omega + i\gamma(n))} + \frac{\omega_{LO}^2 - \omega_{TO}^2}{\omega_{TO}^2 - \omega^2 - i\omega\Gamma}\Big), \quad (6)$$

where $\epsilon_\infty = 12.32$, $\omega_{LO} = 45 \times 10^{12}\, rad/s$ $\omega_{TO} = 40 \times 10^{12}\, rad/s$ $\Gamma = 0.56 \times 10^{12}\, rad/s$.

The plasma angular pulsation $\omega_p(n)$ for the Drude model is a function of the carrier density n which can be written

$$\omega_p(n) = \sqrt{ne^2/(m_{eff}\epsilon_0\epsilon_\infty)}. \quad (7)$$

The damping coefficient is $\gamma = e/(\mu m_{eff})$ where $m_{eff} = 0.024\, m_e$ is the electron's effective mass (with m_e the electron mass in vacuum) and $\mu = 24000\, cm^2.V^{-1}.s^{-1}$ the electronics mobility. Here, we have considered that the InAs layers are slightly doped with silicon, which introduces an intrinsic density $n_0 = 2 \times 10^{15} cm^{-3}$. The total carrier density is thus $n = \delta n + n_0$. As a consequence, the plasma frequency is close to 0.5 THz without any optical pumping. When the pump is turned on, the electronics density increases which shifts the plasma frequency to larger values according to Equation (7).

The optically induced modification of the InAs permittivity is then able to yield a modulation of the transmission of a THz plane wave interacting with the structure. We define the modulation depth as the difference between the THz transmission coefficients when the optical pump is either turned on or off: $M = T_{on} - T_{off}$. These transmission coefficients are computed by actualizing the InAs permittivity inside the structure thanks to Equation (6) and by using again the S-matrix formalism, but in the THz range this time. For example, we consider a single 10 μm thick InAs layer. The transmission spectra obtained when the pump irradiance Φ_0 is null or equal to 10 $W.cm^{-2}$ are shown in Fig. 3a. Without the laser pump, we observe several transmission peaks corresponding to Fabry-Perot resonances. The transmission vanishes between 6 and 7 THz in the Reststrahlen phonon band.

When the pump is turned on, the incoming light is completely absorbed within the InAs layer since the typical penetration length is only about 200 nm. Even though the photocarriers are efficiently photogenerated close to the surface, they diffuse into the whole slab, since the ambipolar diffusion length is much larger than its actual thickness. The photocarrier density being homogeneous, the permittivity at the THz frequency can be considered homogeneous inside the InAs layer. This modification of the permittivity leads to a strong attenuation of the transmission for frequencies lower than 2 THz. The transmission peak around 3.6 THz is smaller and slightly shifted. The optical modification of the InAs permittivity allows one to modulate the THz signal whose maximal modulation depth reaches -0.44 at 0.8 THz, which represents here a 93% relative variation, as shown Fig. 3b. The second modulation peak with $M = -0.37$ is observed at 3.6 THz. The drastic modulation around 1 THz is attributed to an epsilon near-zero absorption mechanism which has already been theoretically and experimentally demonstrated [35]. However, this response, for a single layer, is restricted to a narrow frequency band around 1 THz. In the following, we show that a multilayered structure allows to select the target THz frequency on a wider range or to modulate several well identified frequencies.

2.2. Design of THz modulators with a differential evolution algorithm

The design of efficient and at demand THz modulators based on a multilayered structure as described above is very challenging. There are no rules which can guide the design, as the modulators have a complex response. Obviously, in order to reach the maximum modulation for a set of given THz frequencies, there must be a very large difference between the response of the structure with and without the optical pump. However, the THz response of the structure is controlled by the way the pump is able to penetrate inside the structure, a phenomenon which is controlled by the interferential patterns which appear and are dependent on the geometry. The pump intensity gives the source term in the highly nonlinear transport equation governing the photogeneration process. Finally the electronics density varies strongly with any change in the thickness of the InAs layers. While multi-physics problem can be simulated, as shown above, it is difficult to suggest any design rule. We thus use a global optimization algorithm remotely inspired by sexual evolution, which is particularly suited for photonics problems which are clearly *modular*, in the sense that the different parts of the structure play often a specific role [41]. We follow

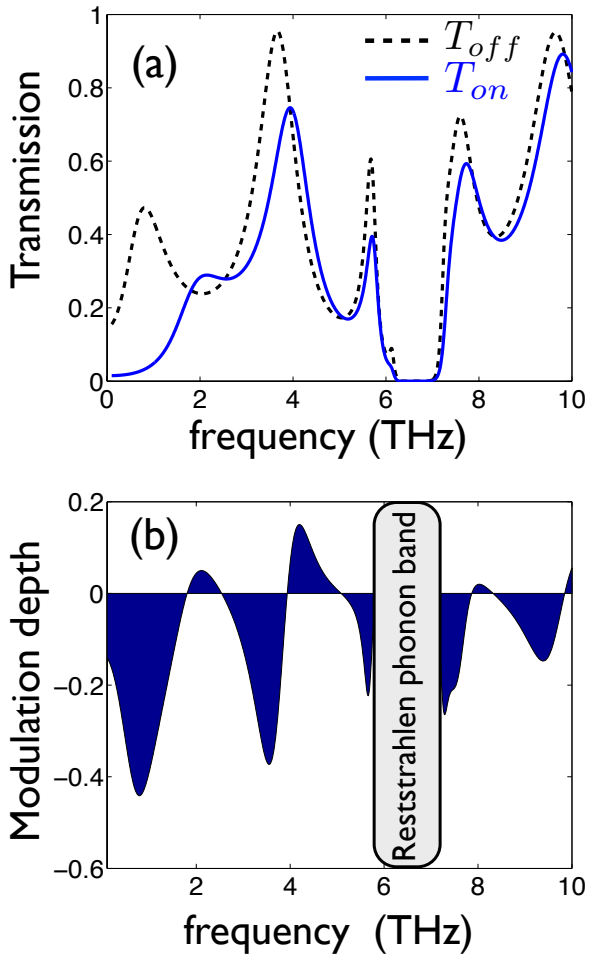

Figure 3. (a) Transmission spectra for a 10 μm thick InAs layer. The solid and dashed lines correspond to the transmission when $\Phi_0 = 10\ W.cm^{-2}$ and when the pump is turn off respectively. (b) Modulation depth M as a function of the frequency.

the same methodology as in [42]. After comparing the most common variants (DE/rand/1, DE/best/1, DE/randToBest/1, DE/currToBest/1, DE/rand/2, and DE/best/2, identified according to the usual classification [36, 43]), we use DE in its current-to-best DE2 version to minimize a cost function which quantifies the targeted functionality. In this framework, each generation is constituted of N_p vectors $\mathbf{x}$. The components of a vector $\mathbf{x}$ are the thicknesses of the GaSb and InAs layers denoted h_j^{GaSb} and h_j^{InAs}. From this set of vectors $\mathbf{x}_n$ $(n = 1, 2, ..., N_p)$ an offspring $\mathbf{v}$ is generated. It combines the difference between two randomly chosen individuals ($\mathbf{x}_{r1}$ and $\mathbf{x}_{r2}$) and the difference between the best individual $\mathbf{x}_b$ for this generation and the vector $\mathbf{x}_n$:

$$\mathbf{v} = \mathbf{x}_n + \alpha(\mathbf{x}_b - \mathbf{x}_n) + F(\mathbf{x}_{r1} - \mathbf{x}_{r2}). \quad (8)$$

To increase the diversity of the population, a mutation process with variable-wise mutation rate CR mixes the genes of the parent and of the offspring. Finally the parent $\mathbf{x}_n$ is replaced by the mutant offspring if the latter lowers the cost function. Our optimizations are performed with a population $N_p = 30$, a mutation probability $CR = 0.8$ and the parameters $\alpha = 0.6$ and $F = 1$. The algorithm is initialized with a random set of $\mathbf{x}_n$ lying in our parameter space (see section 3) and these calculation are made 10 times to be sure that the structure is optimal. Our strategy aims at finding the simplest structure that matches our objective. For this purpose, we consider N pairs of GaSb-InAs layers, Fig. 1. The optimization is performed for an increasing number of N= $\{1, 2, ...\}$ which leads to determine 2N thicknesses. The number of pair of layers is incremented until the cost function of the (N+1)-structure does not outperform that of the (N)-structure. DE systematically converges to the optimal solution since the following structures consist of a number of layers smaller than 20 [42]. We estimate that the accuracy on the thicknesses less than 0.1 μm.

3. Results

In this section we present THz modulators based on GaSb and InAs multilayers designed by DE and which can be deemed interesting. We consider the frequency range 0.5-5 THz and we calculate the modulation depth for a pump irradiance $\Phi_0 = 10\,W.cm^{-2}$. This low value is similar than that utilized in an experimental demonstration of a THz modulator based on an epsilon-near-zero slab [35]. In the following, the maximal thickness for each layer is limited to 10 μm. The structure is illuminated in normal incidence by a plane wave for both infrared and THz radiations.

3.1. Single-frequency THz modulators

3.1.1. 3 THz modulator For many application it is essential to modulate the THz signal at a target frequency. Here, we look for the simplest structure that presents a maximal modulation at a frequency f_0. We choose to optimize the absolute modulation depth rather than the relative modulation depth to get the largest possible variation of the transmission.

The cost function minimized by DE is simply $cost = 1 - |M(f_0)|$ where $M(f_0)$ is the modulation depth calculated at the frequency f_0.

We start with $f_0 = 3$ THz. The modulation depth spectra are calculated for an increasing number of layer pairs, and the results are shown Fig. 4(a-c). The corresponding structures are represented on Fig. 4(d-f) where the real part of the permittivity is calculated at f_0 when the pump is turned on. The incident THz wave progresses from left to right. The optimal 2-layers structure found with DE is made of GaSb and InAs layers of respective thicknesses $h_1^{GaSb} = 9.7$

μm and $h_1^{InAs} = 3\ \mu m$, as shown Fig. 4(d). At 3 THz, an irradiance $\Phi_0 = 10\,W.cm^{-2}$ is not intense enough to obtain a metallic behavior for the InAs layers (*i.e.* a negative permittivity). The modulation depth spectrum shows a peak around 3 THz with $M(f_0) = -0.45$ for $N = 1$. The 4-layers and 6-layers structures ($N = 2$ and $N = 3$) are more resonant since the modulation peak at 3 THz presents a smaller full width at half maximum (FWHM) (see Fig. 4(b,c)).

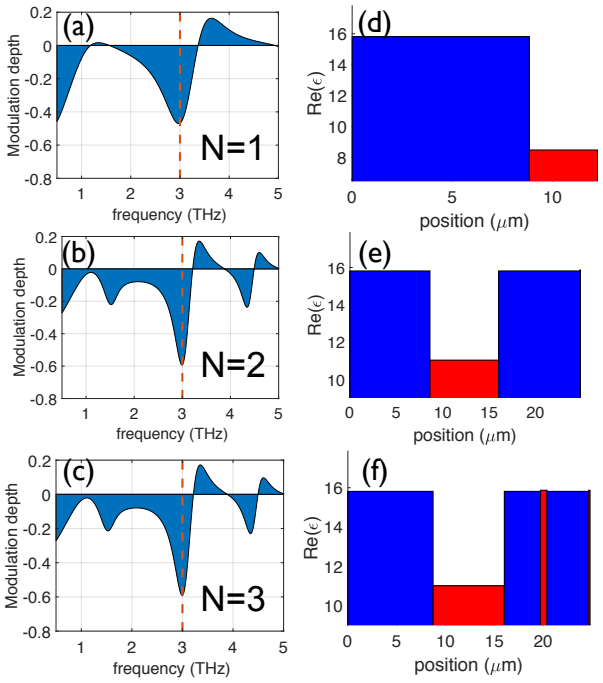

Figure 4. (a-c) Modulation depth as a function of the frequency for a number of GaSb-InAs layer pairs $N = \{1, 2, 3\}$. The target frequency is $f_0 = 3$ THz. (d-f) Real part of the permittivity within the multilayers with $N = \{1, 2, 3\}$ calculated at 3 THz and for $\Phi_0 = 10\,W.cm^{-2}$. The red and blue bars correspond to the InAs and GaSb layers.

The efficiency of the modulator increases as the number of layers increases, as summarized Fig. 5. The modulation depth $M(f_0)$ reaches -0.59 for a 3 and 4 layer pairs. A maximal relative modulation depth $|1 - T_{off}/T_{on}|$ of 63 % is reached. The simplest and efficient THz modulator operating at 3 THz is obtained for N=3 since an additional structuring does not bring any further improvement.

The analysis of the structures obtained for one to three pairs of layers reveals that the two first GaSb and InAs slabs present similar thicknesses about 10 μm and 3 μm respectively, Fig. 4(d,e,f). This pair of slabs is the fundamental building block responsible for the modulation at 3 THz. The additional structuring for larger structures mostly sharpens the resonance and increases the efficiency of the modulator. This behavior proves that our photonics structures are modular.

Furthermore, the transmission spectra calculated for the simplest N=1 structure shows that the transmission is optimized at the resonant frequency when the pump is off Fig. 6. We conclude that DE algorithm first looks for structures that boost the transmission by tailoring a Fabry-Perot resonance at the targeted frequency. Next, when the pump is turned on, the modification of the material properties shifts and lowers the transmission which allows one to get an optimal modulation. The DE algorithm thus indicates that a strategy based on the optimization of the transmission rather than of the absorption, as developed with metamaterials [17, 10, 12, 35], may actually be an efficient strategy.

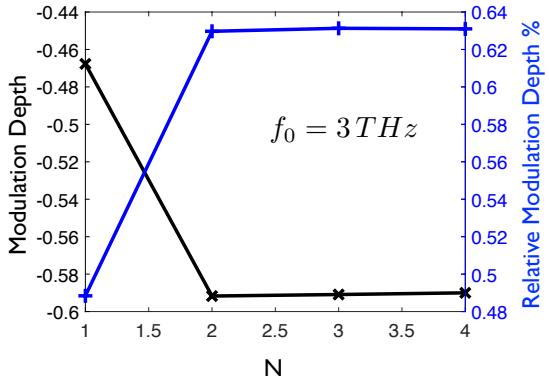

Figure 5. Modulation depth (solid line) and relative modulation depth (dashed line) calculated at 3 THz for an increasing number of GaSb-InAs layer pairs.

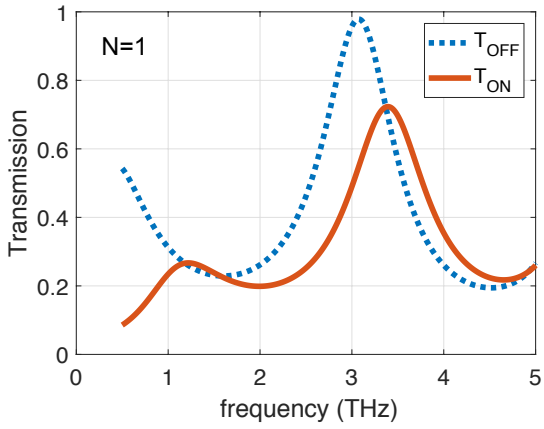

Figure 6. Transmission spectra for the optimal 3 THz modulation presenting N=1 pair of slabs (see Fig. 4 (d)). The solid and dashed lines correspond respectively to the on and off states.

3.1.2. 1 THz modulator The optimized multilayer obtained above is not a general structure that is able to operate at another frequency. For lower frequencies,

a 10 $W.cm^{-2}$ irradiance induces a metallic behavior for the InAs layers which drastically modifies the optimization strategy. For example, let us consider a target frequency $f_0 = 1$ THz. Following the same principle, the optimal modulation depth is plotted as the number of the layer pairs increases in Fig. 7. The modulation is about -0.69 for less than 3 pairs and reaches -0.75 for 5 and 6 pairs. The modulation spectra shows a wide resonant peak around 1 THz for a single pair of GaSb and InAs layers whose thicknesses are respectively 0.02 μm and 1.9 μm, Fig. 8(a). The InAs layer becomes metallic in the THz range when the pump is turned on, with a real part for the permittivity about -45, Fig. 8(c). This metallic slab is placed in front of a multilayer consisting of 5 pairs of layers, Fig. 8(d). We underline that the final structure comes down to a simple bi-layer structure consisting in an InAs layer of 3 μm, followed by a 36 μm GaSb layer. In that case, the 1 THz peak is sharpened and the optimal modulation depth reaches -0.75 (*i.e.* 85 %), as shown Fig. 8(b). Again the first InAs layer is the fundamental building block present in all the optimized 1 THz modulators, another sign that the problem, despite its overall complexity, is still modular.

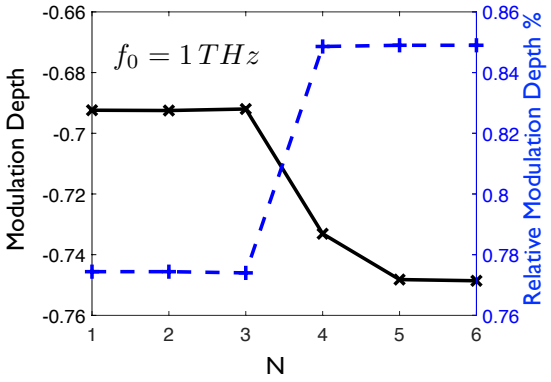

Figure 7. Modulation depth (solid line) and relative modulation depth (dashed line) calculated at 1 THz for an increasing number of GaSb-InAs pair of layers.

One could wonder if that modulator still works whatever the pump irradiance since the photogeneration process directly drives the permittivity profile of the structure. As seen on figure 9, the modulation peaks, and particularly the 1 THz peak, do not shift notably when the pump irradiance changes. The modulation depth varies from -0.36 to -0.78 for an irradiance ranging between 1 and 15 $W.cm^{-2}$. We conclude that the optimized THz modulator is efficient at any pump power with a modulation depth at 1 THz that depends nonlinearly on the irradiance, according to the results shown in Fig. 10.

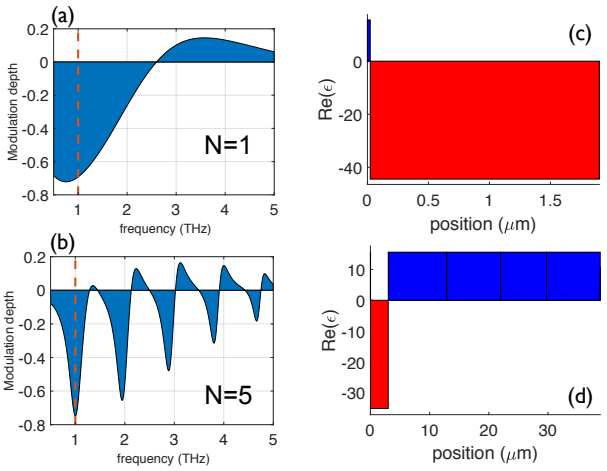

Figure 8. (a-b) Modulation depth as a function of the frequency for a number of GaSb-InAs pair N=1 and N=5. The target frequency is $f_0 = 1$ THz. (C-d) Permittivity maps for the multilayers with N=1 and N=5 calculated at 1 THz and for $\Phi_0 = 10\,W.cm^{-2}$. The red and blue bars correspond to the InAs and GaSb layers.

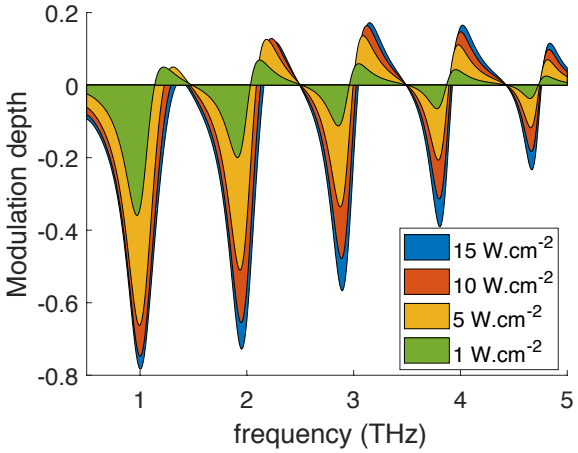

Figure 9. Modulation depth spectra for several pump irradiances for the optimized multilayer with N=5 operating at 1 THz.

3.2. Multi-frequency THz modulators

As seen previously, complex structures actually present several THz modulation peaks. This behavior opens the possibility to design efficient multi-frequency THz modulators. We consider now a set of n_f target frequencies f_i with $i = \{1, ..., n_f\}$. The cost function is defined by $cost = 1 - \frac{1}{n_f}\sum_{i=1}^{n_f} |M(f_i)|$ where the $M(f_i)$ is the modulation depth calculated at the frequency f_i. Here, we look multi-frequency modulators operating at the target frequencies $\{1, 2, 3, 4\}$ THz. The DE algorithm found an optimal structure for N=4 whose modulation spectrum corresponds to the objective Fig. 11 (a). The respective modulation depth are -0.62, -0.56, -0.53, -0.27 from 1 to 4 THz. The thicknesses

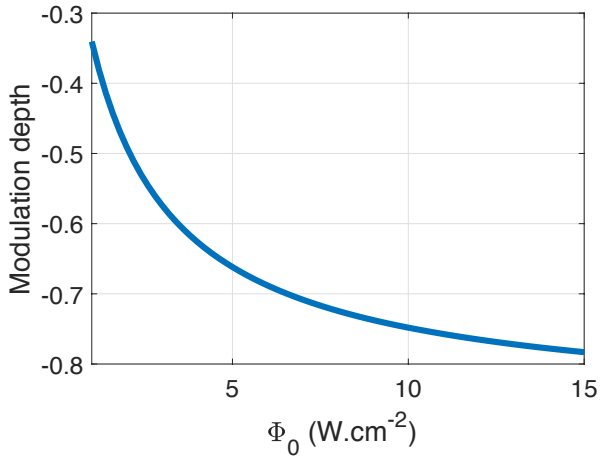

Figure 10. Modulation depth for the optimized multilayer with N=5 operating at 1 THz as a function of the pump irradiance.

of the layers are $h^{GaSb} = \{8.3, 7.2, 3.3, 8.1\}$ μm and $h^{InAs} = \{10, 0, 0.01, 0\}$ μm. Here, we represent the refractive indices of the materials calculated at the infrared frequency since the InAs permittivity changes in the range of 1-4 THz, Fig. 11 (b). By eliminating the layers with a vanishing thickness, the optimal structure simplifies in a 10 μm InAs layer sandwiches between two GaSb layers of thicknesses 8.3 and 18.6 μm.

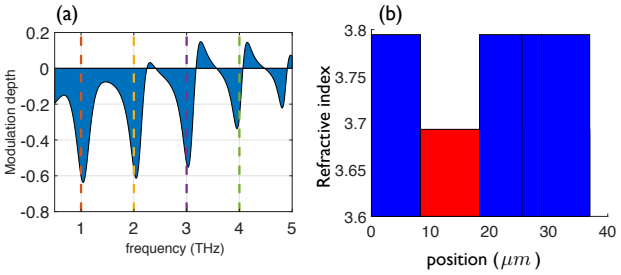

Figure 11. (a) Modulation depth for the optimized multilayer with N=4 operating for the set of target frequencies $\{1, 2, 3, 4\}$ THz. (b) Refractive index at the infrared frequency. The red and blue bars correspond to the InAs and GaSb layers.

Such a multi-frequency THz modulator is not easy to design since both InAs and GaSb are dispersive materials.

To illustrate the efficiency of the DE optimization method, we now chose a set of resonant frequencies $\{1, 3, 4\}$ THz and we impose a minimal modulation at 2 THz. Again DE algorithm found an efficient solution for N=4, Fig. 12 (a). The modulation depths calculated at 1, 3 and 4 THz are respectively -0.57, -0.33, -0.39 while the modulation depth at 2 THz is almost null (-0.04). This novel modulator is now quite different than the previous one, Fig. 12 (b). The thicknesses are $h^{GaSb} = \{7.3, 3.8, 19.1\}$ μm and $h^{InAs} = \{3.5, 2.9\}$ μm. To achieve this non trivial modulator, a GaSb layer of 3.8 μm in now inserts into the InAs layer. These results demonstrate that complex modulation operations can be obtained with a reduced number of layers.

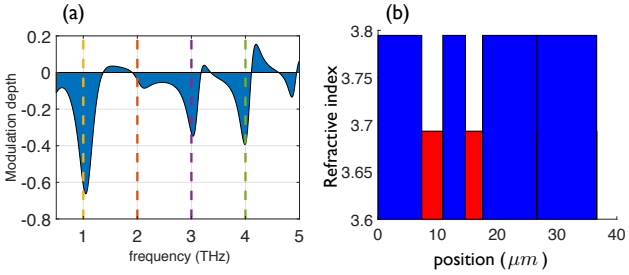

Figure 12. (a) Modulation depth for the optimized multilayer with N=4 presenting a high modulation for the frequencies $\{1, 3, 4\}$ THz and a minimal modulation at 2 THz. The dashed lines correspond to the target frequencies. (b) Refractive index at the infrared frequency. The red and blue bars correspond to the InAs and GaSb layers.

4. Conclusion

We have shown that multilayers alternating GaSb and InAs materials are simple structures which nonetheless allow to conceive optically actuated THz modulators presenting a high efficiency. As the physics of these device is rich and highly nonlinear, we have used a global optimization algorithm, Differential Evolution, to compensate for the lack of design rules in the present case. This algorithm has been able to tackle such a complex multiphysics optimization problem, involving a simultaneous optimization of the spatial extension of optical pump within the structure, of the nonlinear photogeneration process and the management of the THz signal in both on and off states.

This approach has allowed us to design THz modulators operating at single or arbitrary multiple frequencies in the range of 0.5-5 THz. Our results show that the design strongly depends on the desired functionality. However, all the designs are optically understandable. A physical analysis indicates that the DE algorithm targets the transmission rather than the absorption, which is the approach commonly taken in the case of metamaterial modulators. The approach suggested by our analysis could inspire design rules in the future, as this strategy has allowed the algorithm to reach particularly important modulation depths. Feasible multilayers of GaSb and InAs actually present modulation depths up to -0.75 and -0.59, obtained at 1 and 3 THz respectively for a low pump irradiance of 10 $W.cm^{-2}$ in the continuous regime. The proposed structures might be realized using epitaxy techniques such as hydride vapour phase epitaxy. These results clearly open up a route for the realization of cheap,

easy to fabricate and efficient THz modulators with a MHz frequency rate.

Acknowledgments

We wish to acknowledge the support received from the Agence Nationale de la Recherche of the French government through the program "Investissements d'Avenir" (16-IDEX-0001 CAP 20-25) and the IMobS3 Laboratory of Excellence (ANR-10-LABX-0016). AM is an Academy CAP 20-25 chair holder.

5. References

[1] Dhillon S, Vitiello M, Linfield E, Davies A, Hoffmann M C, Booske J, Paoloni C, Gensch M, Weightman P, Williams G *et al.* 2017 *Journal of Physics D: Applied Physics* **50** 043001
[2] Lee Y S 2009 *Principles of terahertz science and technology* vol 170 (Springer Science & Business Media)
[3] Federici J F, Schulkin B, Huang F, Gary D, Barat R, Oliveira F and Zimdars D 2005 *Semiconductor Science and Technology* **20** S266
[4] Tonouchi M 2007 *Nature photonics* **1** 97
[5] Zaitsev K, Chernomyrdin N, Kudrin K, Reshetov I and Yurchenko S 2015 *Optics and Spectroscopy* **119** 404–410
[6] Köhler R, Tredicucci A, Beltram F, Beere H E, Linfield E H, Davies A G, Ritchie D A, Iotti R C and Rossi F 2002 *Nature* **417** 156
[7] Williams B S 2007 *Nature photonics* **1** 517
[8] Belacel C, Todorov Y, Barbieri S, Gacemi D, Favero I and Sirtori C 2017 *Nature communications* **8** 1578
[9] Wang L, Zhang Y, Guo X, Chen T, Liang H, Hao X, Hou X, Kou W, Zhao Y, Zhou T *et al.* 2019 *Nanomaterials* **9** 965
[10] Chen H T, Taylor A J and Yu N 2016 *Reports on progress in physics* **79** 076401
[11] Fan K and Padilla W J 2015 *Materials Today* **18** 39–50
[12] Ma Z, Geng Z, Fan Z, Liu J and Chen H 2019 *Research* **2019** 6482975
[13] Degl'Innocenti R, Kindness S J, Beere H E and Ritchie D A 2018 *Nanophotonics* **7** 127–144
[14] Sautter J, Staude I, Decker M, Rusak E, Neshev D N, Brener I and Kivshar Y S 2015 *ACS nano* **9** 4308–4315
[15] Cui T, Bai B and Sun H B 2019 *Advanced Functional Materials* **29** 1806692
[16] Chen H T, O'hara J F, Azad A K, Taylor A J, Averitt R D, Shrekenhamer D B and Padilla W J 2008 *Nature Photonics* **2** 295–298
[17] Chen H T, Padilla W J, Zide J M, Gossard A C, Taylor A J and Averitt R D 2006 *Nature* **444** 597
[18] Karl N, Reichel K, Chen H T, Taylor A, Brener I, Benz A, Reno J, Mendis R and Mittleman D 2014 *Applied Physics Letters* **104** 091115
[19] Yu S, Wu X, Wang Y, Guo X and Tong L 2017 *Advanced Materials* **29** 1606128
[20] Chen X, Tian Z, Li Q, Li S, Zhang X, Ouyang C, Gu J, Han J and Zhang W 2020 *Chinese Physics B* **29** 077803
[21] Burdanova M G, Katyba G M, Kashtiban R, Komandin G A, Butler-Caddle E, Staniforth M, Mkrtchyan A A, Krasnikov D V, Gladush Y G, Sloan J *et al.* 2021 *Carbon* **173** 245–252
[22] Shrekenhamer D, Rout S, Strikwerda A C, Bingham C, Averitt R D, Sonkusale S and Padilla W J 2011 *Optics express* **19** 9968–9975
[23] Zhang Y, Qiao S, Liang S, Wu Z, Yang Z, Feng Z, Sun H, Zhou Y, Sun L, Chen Z *et al.* 2015 *Nano letters* **15** 3501–3506
[24] Lee G, Nouman M T, Hwang J H, Kim H W and Jang J H 2018 *AIP Advances* **8** 095310
[25] Rout S and Sonkusale S R 2016 *APL Photonics* **1** 086102
[26] Huang Y, Yu Y, Qin H, Sun J, Zhang Z, Li X, Huang J and Cai Y 2016 *Applied Physics Letters* **109** 201110
[27] Okada T and Tanaka K 2011 *Scientific reports* **1** 121
[28] Georgiou G, Tyagi H, Mulder P, Bauhuis G, Schermer J and Rivas J G 2014 *Scientific reports* **4** 3584
[29] Mezzapesa F P, Columbo L L, Rizza C, Brambilla M, Ciattoni A, Dabbicco M, Vitiello M S and Scamarcio G 2015 *Scientific reports* **5** 16207
[30] Georgiou G, Tserkezis C, Schaafsma M, Aizpurua J and Rivas J G 2015 *Physical Review B* **91** 125443
[31] Steinbusch T P, Tyagi H K, Schaafsma M C, Georgiou G and Rivas J G 2014 *Optics express* **22** 26559–26571
[32] Wang X, Xie Z, Sun W, Feng S, Cui Y, Ye J and Zhang Y 2013 *Optics letters* **38** 4731–4734
[33] Yang Y, Kamaraju N, Campione S, Liu S, Reno J L, Sinclair M B, Prasankumar R P and Brener I 2016 *ACS Photonics* **4** 15–21
[34] Alvear-Cabezón E, Smaali R, Centeno E, Gonzalez-Posada F and Taliercio T 2018 *Physical Review B* **98** 035305
[35] Alvear-Cabezón E, Taliercio T, Blin S, Smaali R, González-Posada F, Baranov A, Teissier R and Centeno E 2020 *Applied Physics Letters* **117** 111101
[36] Storn R and Price K 1997 *Journal of global optimization* **11** 341–359
[37] Smaali R, Omeis F, Centeno E, Taliercio T, Gonzalez-Posada F and Cerutti L 2019 *Physical Review B* **100** 041302
[38] Taliercio T, Guilengui V N, Cerutti L, Tournié E and Greffet J J 2014 *Optics express* **22** 24294–24303
[39] Defrance J, Lemaître C, Ajib R, Benedicto J, Mallet E, Pollès R, Plumey J P, Mihailovic M, Centeno E, Ciracì C *et al.* 2016 *Journal of Open Research Software* **4**
[40] Shur M S 1996 *Handbook series on semiconductor parameters* vol 1 (World Scientific)
[41] Barry M A, Berthier V, Wilts B D, Cambourieux M C, Bennet P, Pollès R, Teytaud O, Centeno E, Biais N and Moreau A 2020 *Scientific reports* **10** 1–10
[42] Bennet P, Juillet P, Ibrahim S, Berthier V, Barry M A, Réveret F, Bousquet A, Teytaud O, Centeno E and Moreau A 2021 *Physical Review B* **103** 125135
[43] Price K, Storn R M and Lampinen J A 2006 *Differential evolution: a practical approach to global optimization* (Springer Science & Business Media)